AIAA SciTech Forum
23-27 January 2023, National Harbor, MD & Online
AIAA SCITECH 2023 Forum
10.2514/6.2023-0434

Numerical Simulation of Discrete Co-Flow Jets NACA-6415 Airfoil in Varied Flow Conditions

Zhijin Lei, *Gecheng Zha †
Dept. of Mechanical and Aerospace Engineering
University of Miami, Coral Gables, Florida 33124

Abstract

This paper numerically simulates Co-Flow Jet (CFJ) airfoils using discrete injection jets, which is motivated by the hypothesis that a discrete CFJ (DCFJ) airfoil will generate both streamwise and spanwise vortex structures to achieve more effective turbulent mixing than an open slot CFJ airfoil. An effective open-slot CFJ momentum coefficient C_μ^* is defined for DCFJs. A NACA-6415 airfoil is used as baseline.Two sets of CFD models for open-slot CFJ and DCFJ NACA-6415 wings are used, one simulating the actual rectangular test section in wind tunnel, the other using the far field conditions. All the DCFJ airfoil models are simulated at the experimental flow conditions of freestream Mach number of 0.029, Reynolds number of 2.05×10^5 at a range of angles of attack (AOA) from 0° to 35°. The numerical simulations employ the intensively validated in-house CFD code FASIP, which utilizes a 3-D RANS solver with Spalart-Allmaras (S-A) turbulence model, 3rd order WENO scheme for the inviscid fluxes, and 2nd order central differencing for the viscous terms.

This initial study shows that, at a given C_μ^*, the DCFJ provides extra lift enhancement and drag reduction compared with open slot CFJ airfoil. The DCFJ airfoil can achieve up to a 250% increase of maximum lift, and simultaneously generates a tremendous thrust. The stall angle of attack is also significantly increased. The vortex structure near discrete injection slots are visualized. The numerical simulation confirms the previous experimentation result that the performance improvement brought by DCFJ are at the cost of high energy expenditure compared with the open slot CFJ airfoil. The lift coefficients versus AoA and power coefficients from CFD simulation are in good agreement with the previous wind tunnel experiment.

Nomenclature

CFJ	Co-flow Jet
AoA	Angle of Attack
AR	Aspect Ratio
C_μ	Jet Momentum Coefficient $\dot{m}_j U_j/(q_\infty S_{ref})$
c	Chord Length
DPIV	Digital Particle Image Velocimetry
LE	Leading Edge
M	Mach Number
OF	Obstacle Factor
P	Static Pressure
P_t	Total Pressure
P_tR	Total Pressure Ratio

* Ph.D. Candidate
† Professor, ASME Fellow, AIAA associate Fellow

P_c	Power Coefficient
q	Dynamic Pressure, $= 0.5\,\rho U^2$
s	Half Wingpan
S	Planform Area
SST	Suction Surface Translation
T_t	Total Temperature
TE	Trailing Edge
U	Flow Velocity
$\overline{P}$	Mass-averaged Static Pressure
$\overline{P_t}$	Mass-averaged Total Pressure
l_{duct}	Slot Width
γ	Specific Heat Ratio
λ_{MAX}	Vortex Identification Criterion
η	Pump Efficiency
ρ	Air Density
∞	Free Stream Conditions
$_j$	Jet Value
$_{max}$	Maximum Value
$_{min}$	Minimum Value
$_{mass-av}$	Mass Average Value
$_{inj}$	Value at Injection slot
$_{suc}$	Value at Suction slot

1 Introduction

The CFJ developed by Zha *et al*[1, 2, 3, 4, 5, 6, 7, 8, 9, 10, 11, 12] provides a promising concept to achieve large lift augmentation, stall margin increase, drag reduction and cruise efficiency. In a CFJ airfoil, an injection slot near the leading edge (LE) and a suction slot near the trailing edge (TE) on the airfoil suction surface are created. As shown in Fig. 1, a small amount of mass flow is drawn into the suction duct, pressurized and energized by micro compressor actuators, and then injected near the LE tangentially to the main flow via an injection slot. The whole process does not add any mass flow to the system and hence is a zero-net-mass-flux(ZNMF) flow control.

The turbulent mixing between the jet and the main flow is the fundamental mechanism for CFJ airfoil performance enhancement. The CFJ airfoil may have a 2-dimensional jet mixing along span with coherent vortex structure due to dissimilarity of two jet parameters.

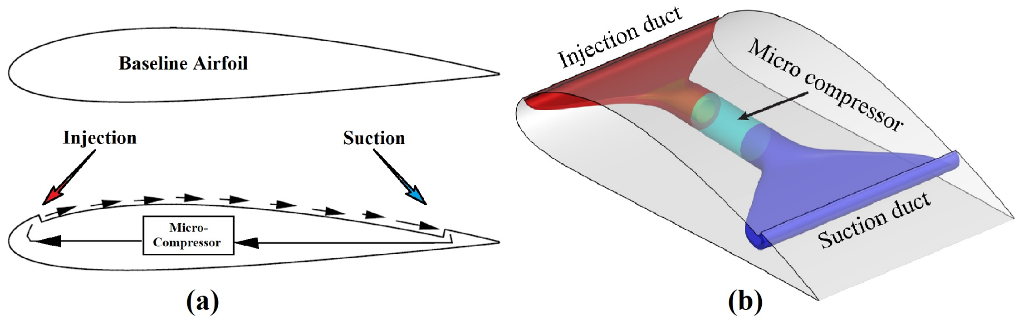

Figure 1: Schematic plot of a conceptual CFJ airfoil(a) and a typical CFJ set(b).

1.1 CoFlow Jet Parameters and Experiment Configuration

A parameter, jet momentum coefficient C_μ, is introduced to quantify the jet intensity, which is defined as:

$$C_\mu = \frac{\dot{m}U_j}{\frac{1}{2}\rho_\infty {U_\infty}^2 S_{ref}} \quad (1)$$

where $\dot{m}$ is the injection jet mass flow rate, U_j is the mass-averaged injection velocity, ρ_∞ and U_∞ denote the free stream density and velocity, and S_{ref} is the planform area of the airfoil.

The power consumption is determined by the jet mass flow and total enthalpy change as the following:

$$P = \dot{m}(H_{t1} - H_{t2}) \quad (2)$$

where H_{t1} and H_{t2} are the mass-averaged total enthalpy in the injection cavity and suction cavity respectively, P is the power required by the micro-compressor actuators and $\dot{m}$ the jet mass flow rate.

The total power can be expressed with the pump efficiency η and total pressure ratio of the pump $\Gamma = \frac{P_{t1}}{P_{t2}}$ as:

$$P = \frac{\dot{m}C_p T_{t2}}{\eta}(\Gamma^{\frac{\gamma-1}{\gamma}} - 1) \quad (3)$$

where γ is the specific heat ratio equal to 1.4 for air, the power coefficient is expressed as:

$$P_c = \frac{P}{\frac{1}{2}\rho_\infty U_\infty^3 S_{ref}} \quad (4)$$

The wind tunnel experiment of open-slot CFJ has provided good match with the theory and numerical results[13, 14, 8]. A CFJ-NACA-6415 test model is made as shown in Fig. 2(a), where rectangular injection and suction cavities displayed in Fig. 2(b) are used, and is tested in the 24-inch x 24-inch wind tunnel depicted in Fig. 2(c). The effect of micro-compressor is simulated by air pumping systems outside the wind tunnel.

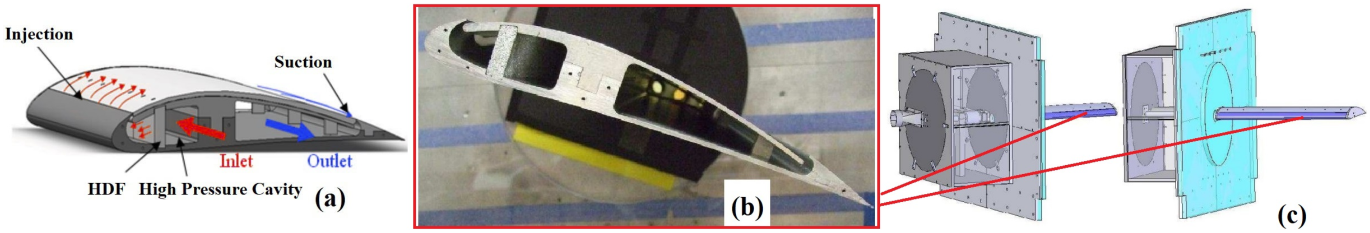

Figure 2: Schematic(a) and profile(b) of an open-slot CFJ wind tunnel test model based on NACA-6415 Airfoil[15]; Schematic of wind tunnel test section[14](c).

1.2 Discretization of an Open-Slot CFJ Straight Wing

Original CFJ configurations use a injection slot throughout the entire wingspan, which is referred as "open-slot injection". Motivated by the hypothesis that a discrete jet will generate both strong streamwise and spanwise vorticity which will produce stronger flow entrainment and mixing, as shown in Fig. 3, Dano[15] uses repeated small tabs to regularly block a certain portion of the injection slot area, as shown in Fig. 4, making the injection flow discrete from each other. Meanwhile, the suction surface (displayed by pink color in Fig. 4) and suction slot (displayed by blue cavity) remain the same. This device is defined as "Discrete CFJ"(DCFJ).

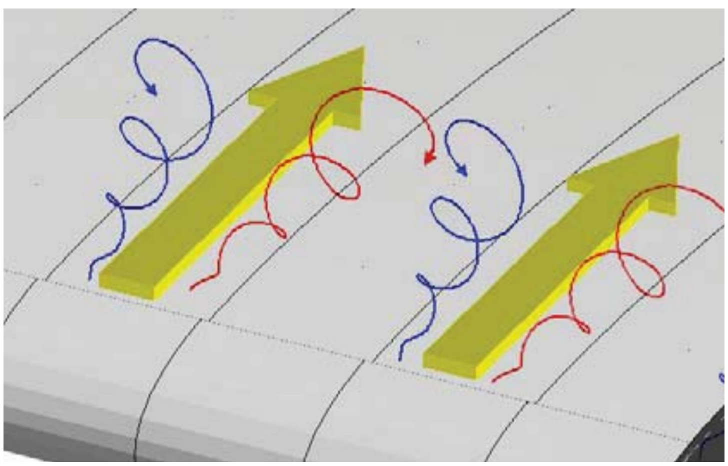

Figure 3: Schematic of hypothesis that a discrete CFJ (DCFJ) airfoil will generate both streamwise and spanwise vortex structures to achieve more effective turbulent mixing than an open slot CFJ airfoil[15].

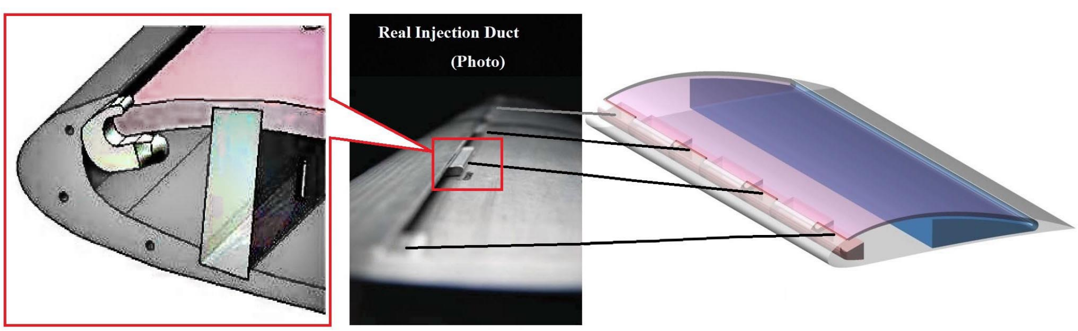

Figure 4: Sketch and photo of Dano's blocking tab(from [14]) on a Discrete CFJ straight wing.

To describe a DCFJ configuration, the concept of obstruction factors (OF) is introduced and defined as the "blocked" area divided by the original CFJ open slot area. For a given mass flow rate, increasing OF will result in an increase in jet exit velocity due to the decrease of jet exit area. Therefore, C_μ will change when OF is changed even if $\dot{m}$ is kept constant. For comparison purposes, Dano [15] defines the jet momentum coefficient for the open-slot CFJ as:

$$C_\mu^* = \frac{\dot{m}U^*{}_j}{\frac{1}{2}\rho_\infty U_\infty{}^2 S_{ref}} \tag{5}$$

where the superscript $*$ stand for open-slot CFJ airfoil. For a given OF, varied configurations can be obtained depending on the number of jet injection holes and the hole sizes. The configurations and C_μ^*s defined by Dano [15] that are used in the following numerical simulation, are shown in Fig. 5.

Name	OF	Config	# of jets	Hole width mm (% cord)	Schematic representation (openings are injection holes, solid lines are tabs)
DCFJ 1/2	1/2	**B**	3	98.4 (16.7%)	
DCFJ 2/3	2/3	**B**	9	21.9 (3.7%)	
DCFJ 3/4	3/4	**B**	5	29.5 (5.0%)	

$\dot{m}$ (kg/s)	C_μ^* and V_{jet} (Open Slot)	$C\mu$ and V_{jet} (Discrete CFJ)				
		DCFJ 1/5	**DCFJ 1/3**	**DCFJ 1/2**	**DCFJ 2/3**	**DCFJ 3/4**
0.030	0.08 (25m/s)	0.11 (29m/s)	0.13 (38m/s)	0.17 (52m/s)	0.23 (73m/s)	0.34 (106m/s))
0.045	0.16 (33m/s)	0.21 (43m/s)	0.23 (51m/s)	0.30 (69m/s)	0.49 (109m/s)	0.67 (153m/s)
0.060	0.30 (46m/s)	0.36 (56m/s)	0.41 (69m/s)	0.58 (97m/s)	0.89 (150m/s)	1.32 (231m/s)

Figure 5: Some discrete CFJ configurations and corresponding C_μs and C_μ^*s from [15].

The wind tunnel airfoil geometry model used for University of Miami's tunnel has a 24-in halfspan and a 12-in chord length, which leads to a blockage of 23.02% at an AoA of 25°, and an even larger blockage of 29.85% at the maximum AoA of 35° used in the experiment, inside the tunnel test section of 24-in × 24-in. This makes the experiment condition differ from actual flight environment and can cause considerable systematic error. However, numerical simulation can provide predictions for both test-section and farfield freestream calculation zones and therefore compare and revise the expected error.

The purpose of research is to numerically simulate the geometry of Discrete CFJs, validate the lift and power results with the experiment, and investigate the mechanism of its lift enhancement effect. Moreover, a hypothesis on CFJ wind tunnel simulation is given that, strong jet flow introduced by CFJ can reduce wind tunnel blockage as well as the experiment result error at high AoAs. This hypothesis will be numerical validated in the simulation.

2 Numerical Algorithms

The in-house high order CFD code Flow-Acoustics-Structure Interaction Package (FASIP) is used to solve the 3D Reynolds averaged Navier-Stokes (RANS) equations. A 3rd order WENO scheme for the inviscid flux [16, 17, 18, 19, 20] and a 2nd order central differencing for the viscous terms [17, 19] are employed to discretize the Navier-Stokes equations. The low diffusion E-CUSP scheme used as the approximate Riemann solver suggested by Zha*etal* [21] is utilized with the WENO scheme to evaluate the inviscid fluxes. Implicit time marching using Gauss-Seidel line relaxation is used to achieve a fast convergence rate [22]. Parallel computing with domain partitioning is implemented to save wall clock simulation time [23]. The FASIP code is intensively validated for CFJ simulations and many steady and unsteady flows [3, 4, 6, 12, 24, 25, 26, 27, 23, 28, 29].

To achieve zero-net mass-flux with the CFJ flow control, the injection mass flow must be equal to the mass flow entering the suction slot. The injection total pressure is iterated to match the same mass flow rate of the suction.

3 Geometry, Boundary Conditions and Mesh

The baseline, open-slot CFJ and all DCFJ geometries sketched in Fig. 5 are based on the wind tunnel model of NACA-6415 airfoil, which is a straight wing with an aspect ratio of 2.0. Only half of the geometry and calculation zone is modelled and meshed to save computation time, and a symmetric plane boundary condition is defined. Two computational domains reflecting wind tunnel test section and farfield freestream respectively are made as shown in Fig. 6(a) and (b) respectively, while both of them meshed using "O-" topology. The surface of CFJ injection slot is based on the shape of actual injection cavity, while the suction slot shape is modified to reduce the separation which does not exist in the suction cavity of the actual model because of the air pumping system.

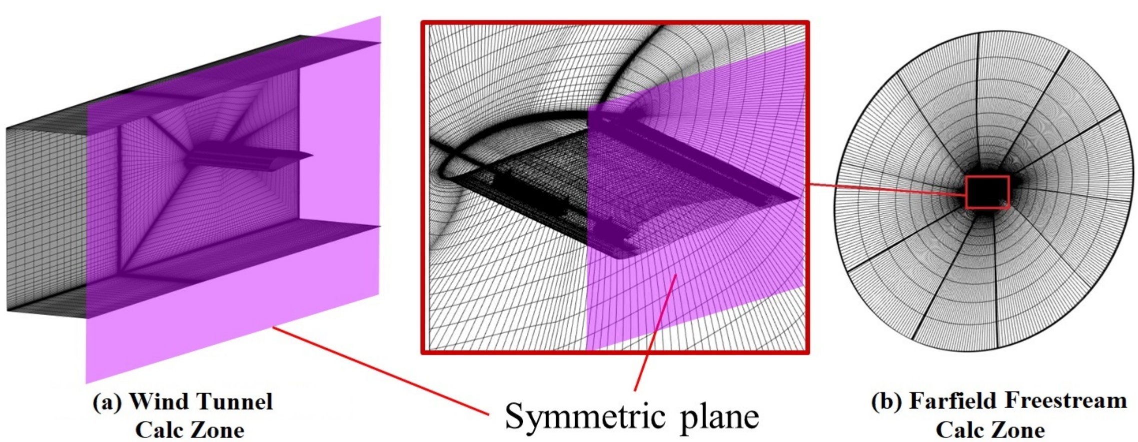

Figure 6: Two meshes used for validation with different calculation zone .

Dimensions and basic characteristics of both types of meshes are given in Table. 1. For the parallel computation, the mesh is split into 150 blocks and the farfield freestream mesh is split into 185 blocks. In all meshes, the first boundary layer spacing on the duct surface is placed to ensure $y+ = 1$.

Total pressure and total temperature are specified at all CFJ duct inlets as boundary conditions. Static pressure is specified at all CFJ duct outlets as boundary conditions. The flow conditions are listed in Table 2 to match Dano's experiment configurations[15].

Table 1: Characteristics of Two Half Model Meshes

Parameter	Farfield	Test Section
Mesh Size	3.02×10^6 Cells	2.68×10^6 Cells
Radius of Farfield Calculation Zone	$50c$	-
Dimension of Test-Section Calculation Zone	-	$4c \times c \times 2c$
Nodes around Airfoil	280	280
Nodes Distributed in Radius Direction of Claculation Zone	60	60
Nodes Distributed along Spanwise Direction on the Wing	100	100
Boundary Layer Spacing	$3 \times 10^{-5}c$	$3 \times 10^{-5}c$

Table 2: Flow Condition

Parameter	Value
M_∞	0.029
Re, based on c	2.05×10^5
C_μ^*, for open-slot CFJ	0.08
C_μ for DCFJ to maintain identical C_μ^*	0.17

4 Results

Two cutaway planes of DCFJ flow field from numerical simulation are presented and compared with DPIV flow visualization results to illustrate the mechanism of performance increasing. Fig. 7 and Fig. 8 shows the difference in flow structure over a tab and along a discrete jet respectively. It can be seen that, the flow over a tab blocking the open slot also appears to be dominated by much stronger turbulent vortices than the flow within the jet plane, which is also dominated by coherent vortices that develop and break down along the suction surface. This effectively increases the turbulent mixing of the wall jets and improved the lift performance[13, 15].

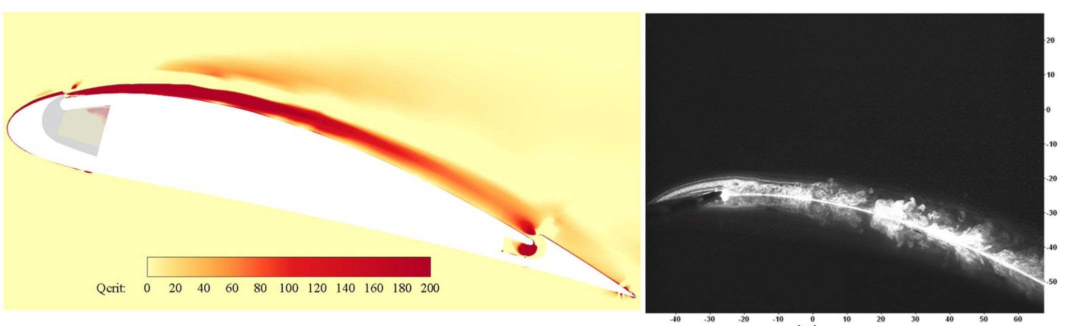

(a) Q-criteria contour over a tab from CFD

(b) Flow visualization from PIV

Figure 7: Visualizations of vortices over a tab of 3/4-DCFJ, AoA=15° and C_μ=0.08, CFJ(a) and wind tunnel experiment(b)[15].

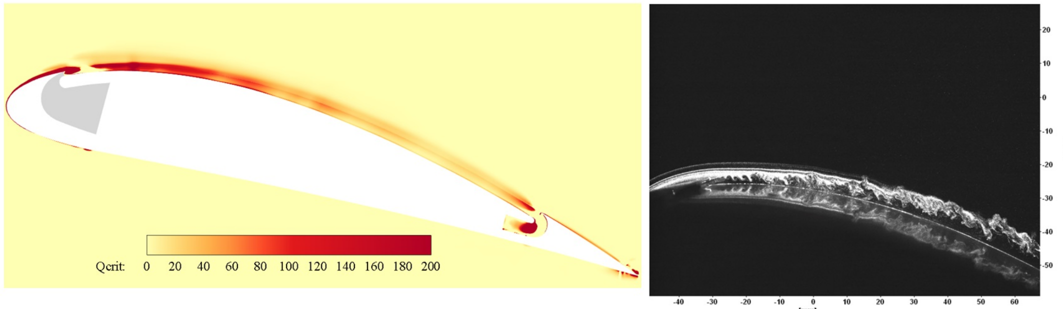

(a) Q-criteria contour over discrete jet from CFD (b) Flow visualization from PIV

Figure 8: Visualizations of vortices over discrete jet of 3/4-DCFJ, AoA=15° and C_μ=0.08, CFJ(a) and wind tunnel experiment(b)[15].

Fig. 9 shows the λ_{MAX}-contoured iso-surface Q-criterion of 2.0 around 2/3-DCFJ, C_μ=0.08, AoA=10° (a) and 3/4-DCFJ, C_μ=0.08, AoA=10°(b). It can be observed that, strong vortex structure near both sides of injection slot can be clearly observed.

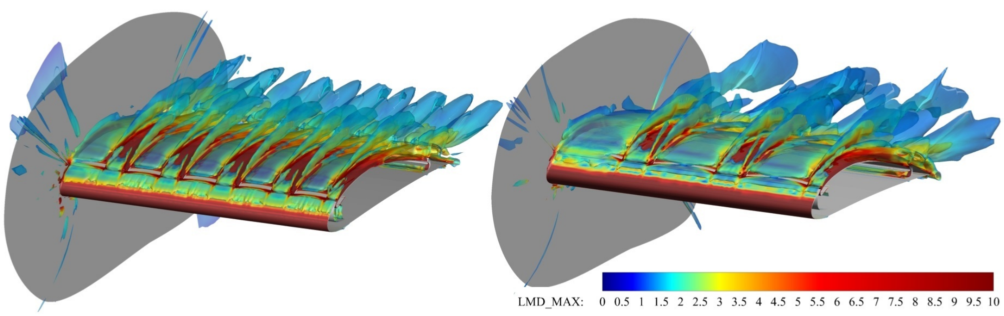

(a) 2/3-DCFJ, *AoA*=10° **(b) 3/4-DCFJ, *AoA*=15°**

Figure 9: Streamlines and Mach number iso-surfaces above the suction surface of open-slot CFJ(a) and 1/2 DCFJ(b).

Lift and drag coefficient C_L for baseline experimental data, baseline CFD data with freestream calculation zone and baseline CFD data with wind tunnel test section calculation zone are grouped together in Fig. 11. It can be observed that, Compared to open-slot CFJ, DCFJ 1/5 and DCFJ 1/3 show a small decrease in lift for all C_μ^* and all AoA except past the stall angle (AoA=25°).

The Comparison of experimental and numerical results of lift and drag coefficients of 1/2 DCFJ, Open-Slot CFJ and a Baseline NACA-6415 Wing Model at AoA=0°, C_μ^*=0.08 are plotted in Fig. 11. It can be seen that the CFD results perfectly matches the experiment.

For DCFJ 1/2, a clear increase in lift can be observed for all AoA. This trend increases for increasing values of C_μ^*. Finally, DCFJ 2/3 and DCFJ 3/4 show a substantial lift increase over the open slot CFJ for all AoA and all C_μ^*.

Evaluation of the lift performance increase for DCFJs compared to baseline and open-slot CFJ are shown in Fig. 11. From Fig. 11 it is evident that the CFJ airfoil is very effective to increase lift, in particular the DCFJ airfoil.

Increasing C_μ^* and OF systematically provides an increase in lift. Notice that, the difference between DCFJ 2/3 and DCFJ 3/4 is not obvious and that, for lift enhancement, they appear approximately equivalent. Compared to the open slot CFJ, the DCFJs only show improvement for OF higher than 1/2. While DCFJ 1/2 show only a 1% increase in lift, DCFJ 2/3 and DCFJ 3/4 show a 30% to 50% increase. These results are considerable considering the magnitude of lift achievable and the energy expenditure of the CFJ pump. For example, using the DCFJ 2/3 at C_μ^* =0.08 provides comparable lift coefficient with the open slot CFJ that needs twice the flow rate. As can be seen in Fig. 11, for open slot CFJ, the maximum lift is increased by 1.5 to 1.8 times. For DCFJ 3/4, the maximum lift is increased by 2.73 times using the same mass flow rate as the open slot CFJ airfoil.

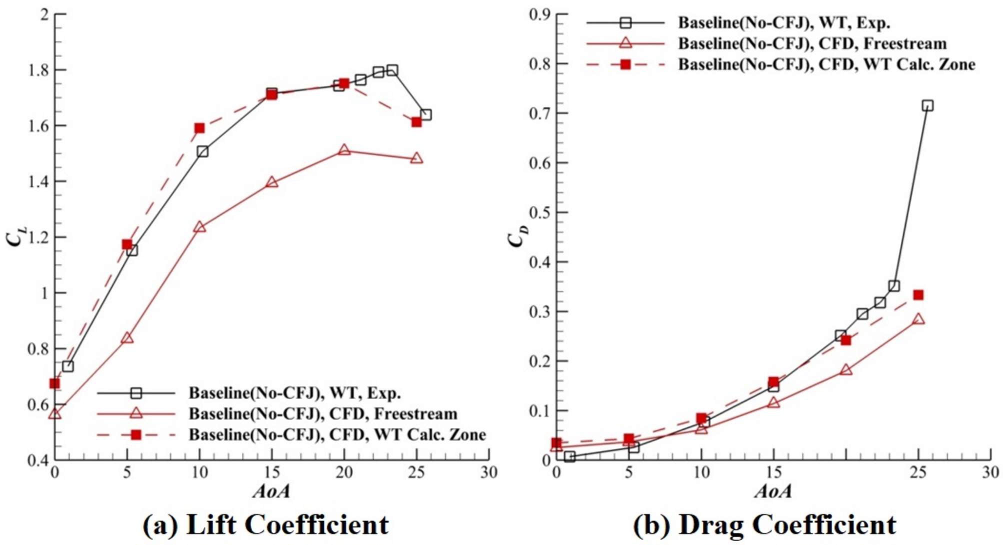

Figure 10: Comparison of Lift Coefficient(a) and Drag Coefficient(b) of the CFD and Experimental Results.

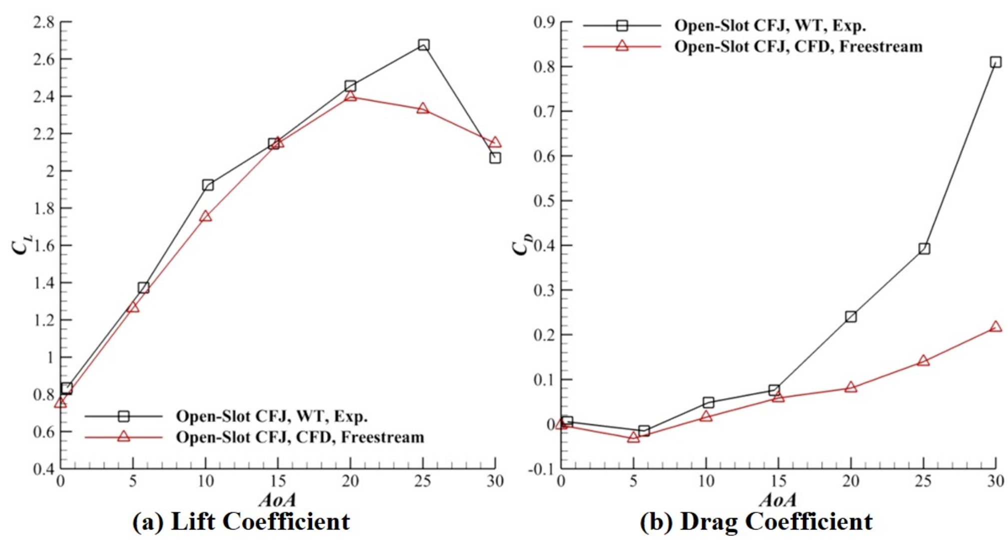

Figure 11: Mach Number Contour around the 1/2 DCFJ-NACA 6421 Airfoil at Injection-Obstructed Region(a) and Injection Slot(b).

Two Mach number contours around the wing profile at spanwise locations with and without injection slot are plotted as shown in Fig. 11. It can be seen that, at the spanwise location where the injection is blocked, there is no obvious separation observed near the trailing edge. This is different from what is found around FDCFJ wings mentioned in Fig. 4. The streamlines shown in Fig. 12(b) around the wing suggests the same conclusion. Also it can be noticed from Fig. 12(b) that, DCFJ provides spanwise forces to the jet flow, and the flow above the suction surface is entraned and mixed as the hypothesis forecasts. At higher AoAs and with larger C_μ^* applied, the list enhancement effect should be observed more clearly.

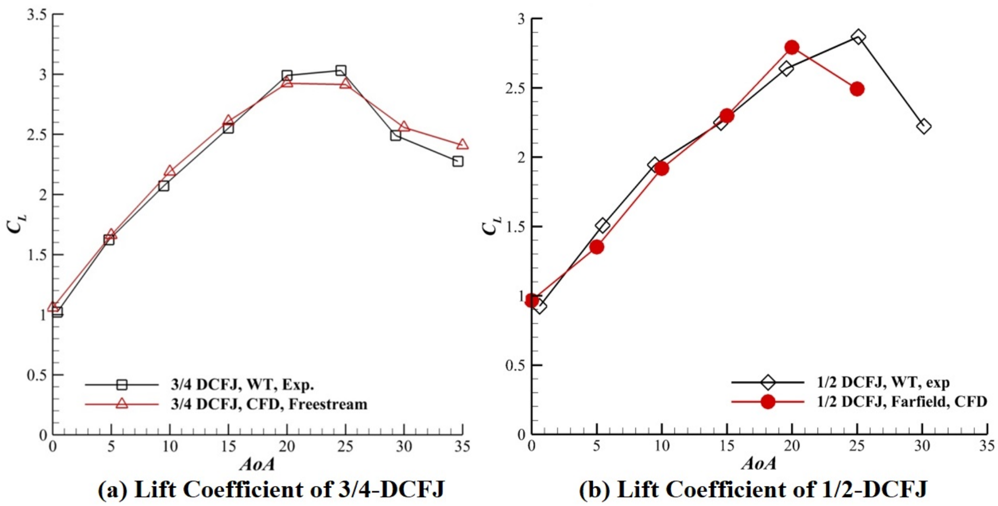

Figure 12: Streamlines and Mach number iso-surfaces above the suction surface of open-slot CFJ(a) and 1/2 DCFJ(b).

Finally, a validation of pressure ratio and power consumptions between experimental result of 2/3-DCFJ Configuration A[15] and CFD result of 2/3-DCFJ Configuration B at varied AoAs, C_μ=0.08 is conducted and the result is plotted in Fig. 13. It can be seen that, despite the difference in tab location distribution, pressure ratio results from experiment and CFD show perfect match, and power consumption results also match with each other closely.

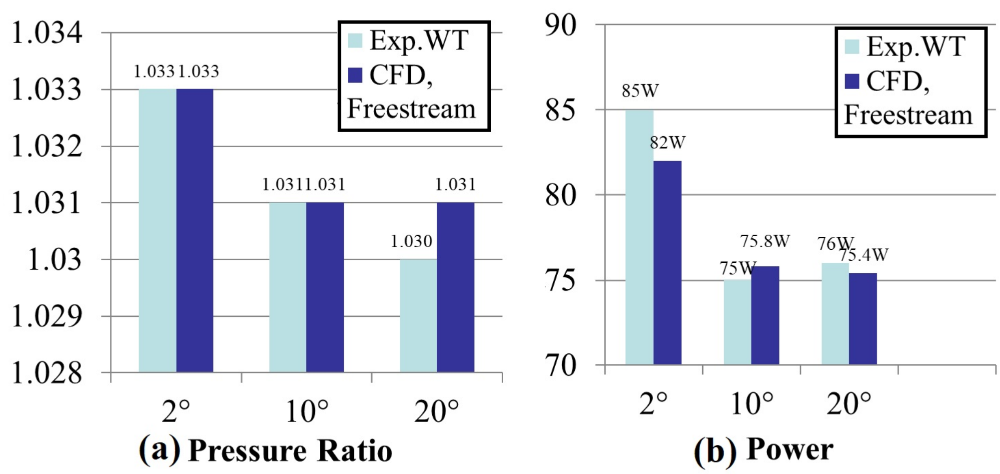

Figure 13: Streamlines and Mach number iso-surfaces above the suction surface of open-slot CFJ(a) and 1/2 DCFJ(b).

5 Conclusions

A Co-Flow Jet (CFJ) airfoil using several configurations of injection jets discretion is numerically simulated motivated by the hypothesis that a discrete CFJ (DCFJ) airfoil will generate both streamwise and spanwise vortex structures to achieve more effective turbulent mixing than an open slot CFJ airfoil. An effective open-slot CFJ momentum coefficient C_μ^* is defined for DCFJs. A NACA-6415 airfoil is used as baseline.Two sets of CFD models for open-slot CFJ and DCFJ NACA-6415 wings are used, one simulating the actual rectangular test section in wind tunnel, the other using the far field conditions. All the DCFJ airfoil models are simulated at the experimental flow conditions of freestream Mach number of 0.029, Reynolds number of 2.05×10^5 at a range of angles of attack (AOA) from $0°$ to $35°$.

This initial study with RANS model shows that, at a given C_μ^*, the DCFJ provides extra lift enhancement and drag reduction compared with open slot CFJ airfoil. The DCFJ airfoil can achieve up to a 250% increase of maximum lift, and simultaneously generates a tremendous thrust. The stall angle of attack is also significantly increased. The vortex structure near discreted injection slots are visualized. The numerical simulation confirms the previous experimentation result that the performance improvement brought by DCFJ are at the cost of high energy expenditure compared with the open slot CFJ airfoil. The lift coefficients versus AoA and power coefficients from CFD simulation are in good agreement with the previous wind tunnel experiment.

6 Acknowledgment

The simulations are conducted on Pegasus super-computing system at the Center for Computational Sciences (CCS) at the University of Miami.

Disclosure: The University of Miami and Dr. Gecheng Zha may receive royalties for future commercialization of the intellectual property used in this study. The University of Miami is also equity owner in CoFlow Jet, LLC, licensee of the intellectual property used in this study.

References

[1] G.-C. Zha and D. C. Paxton, "A Novel Flow Control Method for Airfoil Performance Enhancement Using Co-Flow Jet." *Applications of Circulation Control Technologies*, Chapter 10, p. 293-314, Vol. 214, Progress in Astronautics and Aeronautics, AIAA Book Series, Editors: Joslin, R. D. and Jones, G.S., 2006.

[2] G.-C. Zha, W. Gao, and C. Paxton, "Jet Effects on Co-Flow Jet Airfoil Performance," *AIAA Journal, No. 6,*, vol. 45, pp. 1222–1231, 2007.

[3] G.-C. Zha, C. Paxton, A. Conley, A. Wells, and B. Carroll, "Effect of Injection Slot Size on High Performance Co-Flow Jet Airfoil," *AIAA Journal of Aircraft*, vol. 43, 2006.

[4] G.-C. Zha, B. Carroll, C. Paxton, A. Conley, and A. Wells, "High Performance Airfoil with Co-Flow Jet Flow Control," *AIAA Journal*, vol. 45, 2007.

[5] Wang, B.-Y. and Haddoukessouni, B. and Levy, J. and Zha, G.-C., "Numerical Investigations of Injection Slot Size Effect on the Performance of Co-Flow Jet Airfoil," *Journal of Aircraft*, vol. Vol. 45, No. 6,, pp. pp.2084–2091, 2008.

[6] B. P. E. Dano, D. Kirk, and G.-C. Zha, "Experimental Investigation of Jet Mixing Mechanism of Co- Flow Jet Airfoil." AIAA-2010-4421, 5th AIAA Flow Control Conference, Chicago, IL, 28 Jun - 1 Jul 2010.

[7] B. P. E. Dano, G.-C. Zha, and M. Castillo, "Experimental Study of Co-Flow Jet Airfoil Performance Enhancement Using Micro Discreet Jets." AIAA Paper 2011-0941, 49th AIAA Aerospace Sciences Meeting, Orlando, FL, 4-7 January 2011.

[8] A. Lefebvre, B. Dano, W. Bartow, M. Fronzo, and G. Zha, "Performance and energy expenditure of coflow jet airfoil with variation of mach number," *Journal of Aircraft*, vol. 53, no. 6, pp. 1757–1767, 2016.

[9] A. Lefebvre, G-C. Zha, "Numerical Simulation of Pitching Airfoil Performance Enhancement Using Co-Flow Jet Flow Control," *AIAA paper 2013-2517*, June 2013.

[10] A. Lefebvre, G-C. Zha, "Cow-Flow Jet Airfoil Trade Study Part I : Energy Consumption and Aerodynamic Performance," *32nd AIAA Applied Aerodynamics Conference, AIAA AVIATION Forum, AIAA 2014-2682*, June 2014.

[11] A. Lefebvre, G-C. Zha, "Cow-Flow Jet Airfoil Trade Study Part II : Moment and Drag," *32nd AIAA Applied Aerodynamics Conference, AIAA AVIATION Forum, AIAA 2014-2683*, June 2014.

[12] Lefebvre, A. and Zha, G.-C., "Trade Study of 3D Co-Flow Jet Wing for Cruise Performance." AIAA Paper 2016-0570, AIAA SCITECH2016, AIAA Aerospace Science Meeting, San Diego, CA, 4-8 January 2016.

[13] B. Dano, D. Kirk, and G. Zha, "Experimental investigation of jet mixing mechanism of co-flow jet airfoil," in *5th flow control conference*, p. 4421, 2010.

[14] D. Kirk, *Experimental and numerical investigations of a high performance co-flow jet airfoil.* PhD thesis, University of Miami, 2009.

[15] B. Dano, A. Lefebvre, and G. Zha, "Mixing mechanism of a discrete co-flow jet airfoil," p. 3097, 2011.

[16] Zha, G.C., Shen, Y.Q. and Wang, B.Y., "An improved low diffusion E-CUSP upwind scheme ," *Journal of Computer and Fluids*, vol. 48, pp. 214–220, Sep. 2011.

[17] Shen, Y.Q., and Zha, G.C., "Large Eddy Simulation Using a New Set of Sixth Order Schemes for Compressible Viscous Terms," *Journal of Computational Physics*, vol. 229, pp. 8296–8312, doi:10.1016/j.jcp.2010.07.017, 2010.

[18] Shen, Y.-Q. and Zha, G.-C. and Chen, X.-Y., " High Order Conservative Differencing for Viscous Terms and the Application to Vortex-Induced Vibration Flows," *Journal of Computational Physics*, vol. 228(2), pp. 8283–8300, 2009.

[19] Shen, Y.-Q. and Zha, G.-C. , " Improvement of the WENO Scheme Smoothness Estimator," *International Journal for Numerical Methods in Fluids*, vol. DOI:10.1002/fld.2186, 2009.

[20] Y.-Q. Shen, G.-C. Zha, and B.-Y. Wang, "Improvement of Stability and Accuracy of Implicit WENO Scheme ," *AIAA Journal*, vol. 47, pp. 331–344, 2009.

[21] G.-C. Zha, Y. Shen, and B. Wang, "An improved low diffusion e-cusp upwind scheme," *Computers & fluids*, vol. 48, no. 1, pp. 214–220, 2011.

[22] X.-Y. Chen and G.-C. Zha, "Fully Coupled Fluid-Structural Interactions Using an Efficient High Solution Upwind Scheme." AIAA Paper 2004-2331, to appear in Journal of Fluids and Structures, 2005.

[23] B.-Y. Wang and G.-C. Zha, "A General Sub-Domain Boundary Mapping Procedure For Structured Grid CFD Parallel Computation," *AIAA Journal of Aerospace Computing, Information, and Communication*, vol. 5, No.11, pp. 2084–2091, 2008.

[24] Lefebvre, A. and Dano, B. and Bartow, W. and Di Franzo, M. and Zha, G.-C., "Performance Enhancement and Energy Expenditure of Co-Flow Jet Airfoil with Variation of Mach Number." AIAA Paper 2013-0490, AIAA Journal of Aircraft, DOI: 10.2514/1.C033113, 2016.

[25] Y. Yang and G. Zha, "Super-lift coefficient of active flow control airfoil: What is the limit?," p. 1693, 2017.

[26] G. Z. Kewei Xu, "High control authority 3d aircraft control surfaces using co-flow jet," *AIAA Journal of Aircraft*, vol. DOI 10.1007/s12650-010-0057-7, 2020.

[27] G. Zha, W. Gao, and C.D. Paxton, "Jet Effects on Co-Flow Jet Airfoil Performance," *AIAA Journal*, vol. 45, pp. 1222–1231, 2007.

[28] Liu, Z.-X. and Zha, G.-C., "Transonic Airfoil Performance Enhancement Using Co-Flow Jet Active Flow Control." AIAA Paper 2016-3066, AIAA Aviation, June 13-17 2016.

[29] Lefebvre, A. and Zha, G.-C. , "Design of High Wing Loading Compact Electric Airplane Utilizing Co-Flow Jet Flow Control." AIAA Paper 2015-0772, AIAA SciTech2015: 53nd Aerospace Sciences Meeting, Kissimmee, FL, 5-9 Jan 2015.